Density Functional Study of the Neutral Hypoxanthine Tautomeric Forms

María Eugenia Costas*

Facultad de Química, Universidad Nacional Autónoma de México, México 04510, Distrito Federal, México

Rodolfo Acevedo-Chávez

Centro de Química, Instituto de Ciencias, B. Universidad Autónoma de Puebla, Apartado Postal 1613, Puebla, Puebla, México

Received: February 19, 1997; In Final Form: May 21, 1997[⊗]

The energetic stability and structural and electronic properties of all the ketonic and enolic tautomers of neutral hypoxanthine are studied at the level of density functional theory. We also study the influence of temperature on the tautomeric equilibria and the IR vibrational spectrum of this heterocycle in the gas phase in terms of the contributions of several tautomers. We found that the two N(1)−H ketonic tautomers of hypoxanthine are the energetically most stable ones and represent the main contribution to the experimental IR spectrum. The calculated properties and the potential chemical behavior suggested for hypoxanthine from the theoretical study are in remarkable agreement with the experimental data reported up to date.

I. Introduction

Heterocycles that show in their structure the pyrimidinic ring fused to azolic moieties are interesting systems from the biochemical, pharmacological, chemical, and physicochemical points of view.[1] Among these heterocycles, hypoxanthine (Figure 1) is found as a minor purine base in transfer RNA.[1b] In the purines catabolism, it is a substrate of the metalloenzyme xanthine oxidase in the production of uric acid.[1b] Several studies have been carried out about its interactions with Lewis acids;[1d,2] from them, the N atoms are the favorable metallic coordination sites, the nature depending on the experimental conditions. For the neutral coordinated hypoxanthine, two ketonic tautomeric forms have been detected experimentally,[3] the N(1)−H/N(9)−H and the N(1)−H/N(7)−H, which have also been suggested as the predominant tautomers in aqueous and dimethyl sulfoxide (DMSO) solutions.[4]

With regard to the hypoxanthine tautomerism, an influence of the medium dielectric constant on the equilibrium shift between the N(1)−H/N(7)−H and N(1)−H/N(9)−H ketonic forms has been inferred from experimental and theoretical studies[5] (*e.g.*, N(1)−H/N(9)−H is the predominant tautomer in aqueous solutions; N(1)−H/N(7)−H is the slightly predominant form in DMSO medium). From these studies, the shift of the tautomeric equilibrium in a polar medium toward the tautomer with the highest electric dipole moment in the gas phase is deduced.

To our knowledge, there are no detailed experimental studies about the existence of hypoxanthine enolic tautomers in solution, although it is difficult to discard both its presence in solution with solvents of different dielectric constants and the influence which they could have in the kinetic and thermodynamic stabilities of the physicochemical processes carried out by hypoxanthine in those media.

Although the two N(1)−H ketonic tautomers with prototropic tautomerism in the imidazolic ring appear to be the preponderant species of neutral hypoxanthine in solution at room temperature, the tautomeric equilibria are more complicated in the gas phase because they depend on the temperature conditions. In this respect, the majority of the previous theoretical studies have focused on some electronic properties of only the two energetically most stable ketonic tautomeric forms of hypoxanthine.[4a,6−12] Theoretical studies considering some enolic tautomers of hypoxanthine in the calculation of a specific property are very scarce,[13,14] and only at the semiempirical level. A very recent theoretical study[15] employing several levels of theory has calculated the energetic stability of the tautomers in the gas phase and in the presence of a solvent, however, without exploring the electronic properties of the tautomeric forms and without comparing them with the experimental data available.

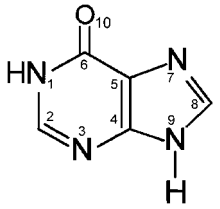

Figure 1. Schematic drawing and numbering sequence of hypoxanthine in its N(1)−H/N(9)−H ketonic tautomeric form.

Here, we present a detailed theoretical study at the DFT level of the energetic stability, and the structural and electronic properties of several ketonic and enolic tautomers of hypoxanthine. We also analyze the influence of temperature on the tautomeric equilibria. The IR vibrational spectrum of hypoxanthine in the gas phase is studied in terms of the contribution of several tautomers.

II. Methods

Geometry optimizations and molecular and electronic properties calculations of the 14 possible tautomers of neutral hypoxanthine were performed at the level of density functional theory with the Becke−Perdew functional[16,17] and the DZVP basis set,[18] using the standard procedure in Gaussian 94.[19]

The crystalline structure[20] of hypoxanthine in its N(1)−H/N(9)−H ketonic tautomeric form was used as starting data for its geometry optimization. This optimized structure was used to construct the initial geometry for other tautomers, by changing the hydrogen atoms to new possible positions on the molecular plane. For the enolic tautomers, a number of initial configurations for the OH group were proposed, and the cis- and trans-forms were always converged to the same structure. Criteria for geometry optimization and self-consistent field (SCF)

[⊗] Abstract published in *Advance ACS Abstracts,* September 15, 1997.

S1089-5639(97)00621-X CCC: $14.00

TABLE 1: Energy Differences Relatives to Tautomer K17 Calculated with the BP Functional and the DZVP Basis Set[a]

tautomer	ΔE (kcal/mol)
K19	0.84, 0.90,[b] 0.80[c]
E9c	5.92, 1.90,[b] 2.80[c]
E9t	7.17, 3.10,[b] 4.30[c]
K37	7.65, 7.20,[b] 6.70[c]
E7c	8.31, 4.20,[b] 5.30[c]
E3t	14.22
E3c	15.53
E7t	17.14
K13	19.29
E1t	20.48
K39	21.29, 21.10,[b] 20.20[c]
K79	23.04
E1c	31 13
K19cr	65.00

[a] K = ketonic, E = enolic, c= cis with respect to N(1), t = trans with respect to N(1), cr = crystalline structure. Numbers represent the positions of the N-protonated atoms shown in Figure 1. [b] Values from ref 15 at the MP2 (6-31+G(d,p)//HF/6-31G(d) level. [c] Values from ref 15 at the DFT (B3LYP, 6-31+G(d,p)//HF/6-31G(d)) level.

convergence were 10^{-7} hartree/bohr and 10^{-9} hartree, respectively. Frequency calculations were done to determine the nature of the stationary points found by geometry optimizations. All the tautomers were stationary points in the geometry optimization procedure, and none showed imaginary frequencies in the vibrational analysis.

All the optimized geometries were used to perform single-point calculations with Gaussian-92[21] with the same functional and basis set, in order to visualize the properties as the electric dipole moment vector, the molecular electrostatic potential, the total electronic density, and the molecular orbitals. The difference in the SCF energy with respect to the value obtained with Gaussian 94 was of 10^{-8} hartree in all cases. Visualization of the several calculated properties was done with the Unichem program.[22] Single-point calculations with the Dgauss program[23] for the Gaussian 94 optimized geometries were also done to obtain the Mayer valence indices.[24]

The calculated frequencies (as wavenumbers) of the IR vibrational spectra were corrected with a scaling factor of 0.9938, which was obtained by comparing the theoretical IR wavenumber of the ν(C═O) vibrational mode (1756.8469 cm^{-1}) for formaldehyde in gas phase (calculated with the same functional, basis set, and methodology as the one used for hypoxanthine) with the experimental value (1746 cm^{-1}). Assignment of the vibrational normal modes for the different tautomers was done by visualizing them at each frequency value with the XMol 1.3.1 program. Frequency calculations were done at 11, 298.15, and 480.15 K to obtain the Gibbs free energy thermal corrections, which were used to calculate the tautomeric equilibrium constants at these temperatures. Vertical first ionization potentials and first electron affinities were obtained by calculating the SCF energy of the monocationic and monoanionic radicals at the optimized structures of the respective neutral tautomers.

The calculations were done on a CRAY YMP4/464 supercomputer (at DGSCA, UNAM), a SGI Power Challenge computer (R8000-18) (at UAM- Iztapalapa) and a SGI workstation (R4400) (at FQ-UNAM).

III. Results and Discussion

A. Energetic Stability. Table 1 shows the differences in energy (kcal/mol) relative to the N(1)−H/N(7)−H tautomer for each one of the ketonic and enolic tautomers of neutral hypoxanthine (K = ketonic, E = enolic; the numbers indicate the protonated N atoms according to the numbering shown in Figure 1). We also include the energy difference for the N(1)−H/N(9)−H ketonic form in its crystalline structure (K19cr) (a single-point calculation).

From these results, the N(1)−H/N(7)−H and N(1)−H/N(9)−H ketonic tautomers are the most stable ones, the last being slightly (0.84 kcal/mol) less favorable. The higher energetic stability of the N(1)−H ketonic forms of hypoxanthine arises, and this is the same behavior deduced from experiments of this heterocycle in solution, as has been pointed out before. The two N(9)−H enolic forms (with the H atom of the OH group in cis- or trans-configuration with respect to the N(1) atom) follow in decreasing stability. Of these, the *cis*−N(9)−H enolic tautomer is relatively more stable; this allows us to suspect a higher basicity of N(1) with respect to N(7). From the stability of these four tautomers, the major role played by the basicity of the N(1) and O(10) atoms may be suggested. The ketonic form N(3)− H/N(7)−H and the *cis*−N(7)−H enolic tautomer follow in energetic stability. For the first one, the lower basicity of N(3) with respect to N(1) can be inferred. For the second one, it is possible to suggest the influence that the deprotonation of the N(9) atom has on the tautomer energetic stability.

With respect to the other eight tautomers, the remarkable increasing energetic instability can be associated with the presence of the two interchangeable H atoms in the same heterocyclic fragment (pyrimidinic or imidazolic ring), or in different rings but with a disposition that produces considerable repulsive interatomic interactions. Finally, the N(1)−H/N(9)−H ketonic tautomer in its crystalline structure is the most unstable one: this points to the great influence that the interactions in the crystalline lattice play in the stabilization of that structure—these interactions are absent in the gas phase.

Table 1 also shows the energy differences relative to the N(1)− H/N(7)−H tautomer reported in ref 15, obtained with both the (b) MP2 and (c) DFT(B3LYP) methods. In that study, the tautomers energetic stability sequence is slightly different as the one we get, but there some tautomers were discarded from the final analysis because the difference of energy determined by semiempirical calculations with respect to the most stable tautomer was very big. Here, we made the complete analysis using the same method for all the tautomers, and the sequence was determined at the same level of theory. Nevertheless, the four most stable tautomers we found are the same as the ones they report. As can be seen in this table, small differences are found between the results determined from calculations at MP2 and DFT levels, and the results we present here (for the six most stable tautomers, ΔE < 10 kcal/mol in all the methods). This comparison may indicate that less expensive methods, such as the DFT we used, are good alternatives to the ab initio calculations. This can support the relative stabilities of the tautomers we present, and allows us to analyze some of their structural and electronic properties with a good confidence. In what follows, only the first six most stable tautomeric forms are considered in the study of their structural and electronic properties, as the energy differences relative to the N(1)−H/N(7)−H tautomer are less than 10 kcal/mol.

B. Structural Parameters. For the two most stable N(1)−H ketonic tautomers, a double bond character for some regions can be inferred. For N(1)−H/N(7)−H these are C(2)−N(3), C(8)−N(9), C(4)−C(5), and C(6)−O(10). For N(1)−H/N(9)−H, they are C(2)−N(3), N(7)−C(8), C(4)−C(5), and C(6)−O(10). Noticeable differences arise for the N(9)−H enolic forms. For the cis-isomer, the internuclear distances let us

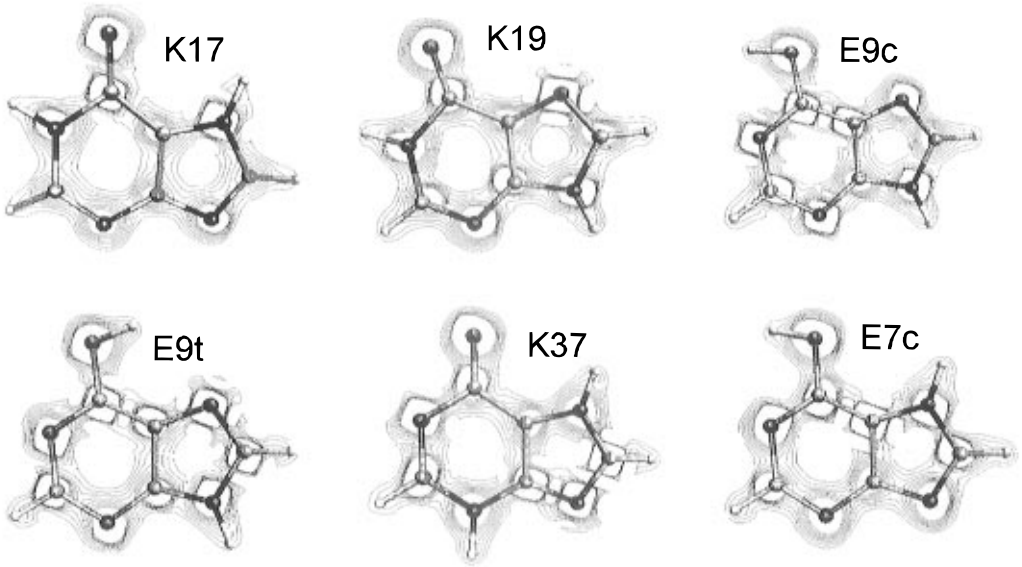

Figure 2. Total electronic charge density contour maps (0.15−0.50 *e*/Å^3 range, changes in 0.05 units) at the molecular plane level for the six most stable tautomers.

suggest a higher delocalization of the electronic density in the pyrimidinic ring. A double bond character is associated with N(7)−C(8) and C(6)−O(10), although the last one shows a lower character of that type with respect to the two ketonic forms mentioned above. An analogous behavior for the 5- and 6-membered rings, and for the C(6)−O(10) is observed for the trans-isomer.

The N(3)−H/N(7)−H tautomer shows a double bond character associated with N(1)−C(2), C(4)−C(5), C(8)−N(9), and C(6)−O(10). Finally, the *cis*−N(7)−H enolic form shows a relative double bond character for C(2)−N(3), C(5)−C(6), C(6)−N(1), and C(8)−N(9). From the data, a relation between the positions of the interchangeable H atoms and the internuclear distances is observed.

With regard to the angles of the CNC groups in the imidazolic ring and for the six tautomers, those N-protonated CNC groups always show higher angles than the deprotonated ones. This could be associated with a higher sp^2 character for the atomic orbitals of the protonated N atoms, and a higher *p*-contribution in the corresponding atomic orbitals of the deprotonated N atoms. For the pyrimidinic ring, this same structural pattern is observed in the N(1)−H/N(7)−H and N(1)−H/N(9)−H tautomers. The N(3)−H/N(7)−H tautomer shows a different behavior: the angle of the N-protonated C(2)−N(3)−C(4) group (117.03°) is lower than the one for the N-deprotonated C(2)−N(1)−C(6) group (120.95°). However, in analyzing the behavior of the CNC group which involves the N(3) atom, it systematically shows lower angles than those of the CNC group that contains the N(1) atom when both groups are deprotonated; the first shows an increase of the angle under protonation. In consequence, the same assumption about the N atoms p-type atomic orbitals contribution in the protonation/deprotonation processes carried out and involving the pyrimidinic ring can also be considered here. The angle of the N(1)−C(6)−C(5) group systematically shows higher values when the tautomers are in enolic form. In these, the C(6)−O(10)−H angles (104.99°−106.90°) let us suggest a noticeable sp^3-character for the O atomic orbitals.

Finally, with respect to the planarity of the structures for the tautomers analyzed, the dihedral angles are almost all 0.01° lower than 80 ± 0.01° reflecting the essentially planar nature of the heterocyclic networks. The analysis let us consider the existence of very small out-of-plane character of the H atoms in some cases.

C. Total Electronic Charge Density. Figure 2 shows the total electronic charge density contour maps (0.15−0.50 *e*/Å^3 range, changes in 0.05 units) in the molecular plane level for the six tautomers here studied. For each tautomer at the 0.15 level, electronic communication in all the molecule is observed. However, for higher values of the electronic density, noticeable differences arise. The N(1)−H/N(7)−H and N(1)−H/N(9)−H tautomers show electronic communication in the following groups: C(2)−N(3), C(4)−C(5), C(8)−N(9) and C(6)−O(10) (for the first one) and C(2)−N(3), C(4)−C(5), N(7)−C(8), and C(6)−O(10) (for the second one). This supports the suggestion made before about the existence of a double bond character in these groups.

For the N(9)−H enolic tautomers, the same analysis let us consider a higher delocalization of the electronic density in the 6-membered ring. The C(6)−O(10) group is associated with a lower double bond character. In the imidazolic moiety, the N(7)−C(8) group is supposed to show in both cases a double-bond character. For these two tautomers, the contour maps are also in agreement with the results discussed before related to the internuclear distances.

A double bond character for the N(1)−C(2), C(4)−C(5), C(8)−N(9) and C(6)−O(10) groups is also supported for the N(3)−H/N(7)−H tautomer. Finally, for the *cis*−N(7)−H enolic tautomer the same character is supported for the C(2)−N(3), C(5)−C(6), C(6)−N(1), and C(8)−N(9) groups; the C(6)−O(10) group shows a lower level of a double bond character.

Upon the consideration of both the internuclear distances and the contour maps and comparing them to the values of the Mayer valence indices[24] for each atom of the tautomers, noticeable agreement both for the structural and potential physicochemical meaning is obtained, supporting again the structural properties and electronic distribution discussed before. For example, for the N(1)−H/N(7)−H tautomer, the Mayer valence indices (N(1), 3.28; C(2), 3.97; N(3), 3.21; C(4), 4.00; C(5), 3.83; C(6), 4.23; N(7), 3.36; C(8), 3.95; N(9), 3.14; O(10), 2.21) are in agreement with the double bond character for the C(2)−N(3), C(4)−C(5), C(8)−N(9), and C(6)−O(10) groups.

D. Molecular Electrostatic Potential and Electric Dipole Moment. Figure 3 shows the contour maps of the molecular electrostatic potential in the molecular plane (0 to −50 kcal/mol range, with changes in 10 units, and with a positive charge as a probe), together with the electric dipole moment vector

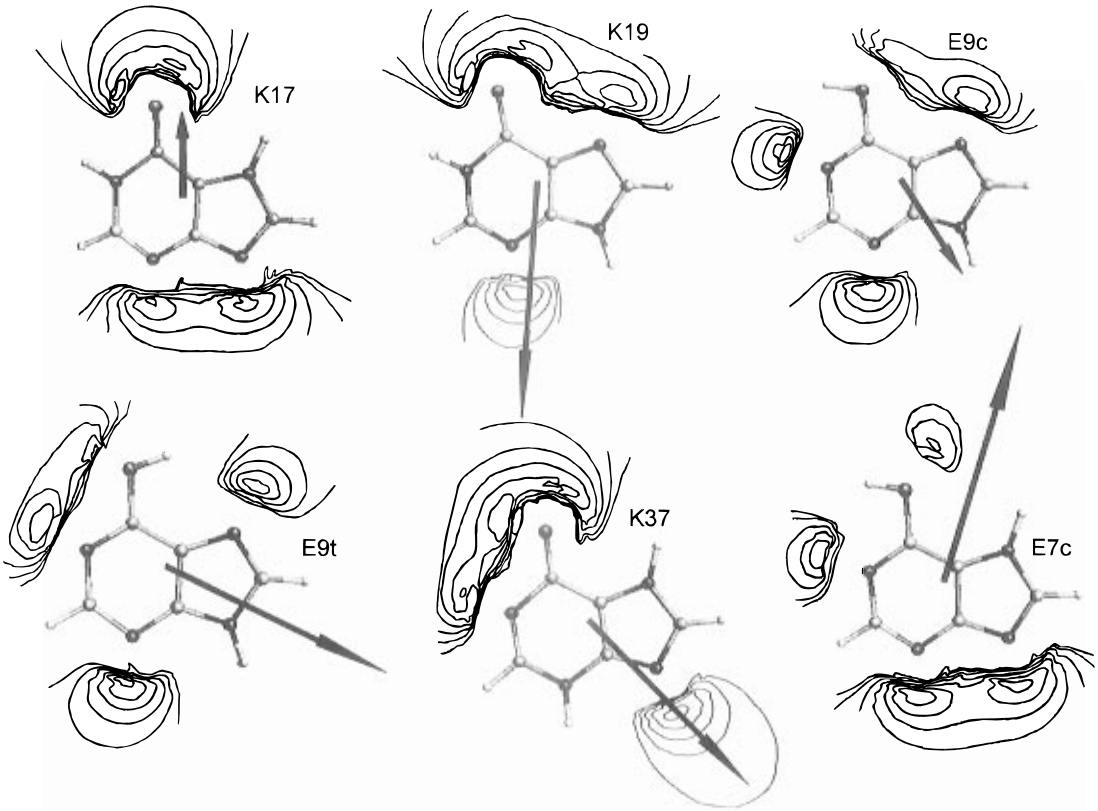

Figure 3. Negative molecular electrostatic potential contour maps (0 to −50 kcal/mol range, with changes in 10 units, considering a positive charge as probe), together with the electric dipole moment vector (the head of the arrow pointing to the positive end) for the six most stable tautomers.

TABLE 2: Dipole Moment Values, HOMO and LUMO Energies and the First Vertical Ionization Potential and First Vertical Electronic Affinity for the Six Most Stable Tautomers

tautomer	μ (D)	HOMO (eV)	LUMO (eV)	I.P. (eV)	E.A. (eV)
K17	1.80, 2.78[a]	−6.00	−2.13	8.73	0.50
K19	5.19, 6.26[a]	−5.84	−2.13	8.55	0.52
E9c	2.52	−6.17	−2.10	8.88	0.48
E9t	4.77	−6.25	−2.19	8.97	0.40
K37	3.92	−5.71	−2.20	8.66	0.37
E7c	5.16	−6.25	−2.21	9.05	0.41

[a] Values from ref 8.

(the arrow pointing to the positive end) for each one of the six most stable tautomers. The values of this property are shown in Table 2.

For the N(1)−H ketonic tautomeric forms the most negative electrostatic potential level lies upon two regions near the O(10) atom and a region near each of the deprotonated N atoms. In both tautomers the protonated regions are associated with positive electrostatic potentials. For these two tautomers the value and direction of the electric dipole moment into the plane are in full agreement with the spatial distribution of the negative and positive electrostatic potential around the heterocycles.

Calculations of the electric dipole moment at the semiempirical level show the same trend (Table 2) as the one we get for the two most stable tautomers.[8] On the other hand, the experimental value (3.16 D in acetic acid[8]) lies between the two values obtained for the N(1)−H ketonic forms; this allows us to suspect that the two tautomers might be present in solution in different molar ratios, depending on the solvent used.

For the N(9)−H enolic tautomeric forms, a similar pattern for the negative potential around the C(2)−N(3)−C(4) fragment is observed. In contrast, the N(1) deprotonated atom in the cis-isomer is associated with a more localized level of the most negative potential. The configuration of the H atom bonded to O(10), influences in a great manner the characteristics of both the negative and positive electrostatic potentials pathways: the 2-D maps clearly show differences in the "channel" of the positive potential around the OH group. As for the above two ketonic tautomers, the protonated regions are associated with positive electrostatic potentials.

The pattern of the negative electrostatic potential for the N(3)−H/N(7)−H shows noticeable differences with respect to the N(1)−H/N(7)−H tautomer. For the first, the O(10) and the N(1) atoms are associated with very localized negative electrostatic potential; for the N(9) atom the most negative potential level is more localized than the one for the same atom in the N(1)−H/N(7)−H tautomer, which suggests the role that the protonated N(3) atom plays. The negative potential for the OH group in the *cis*−N(7)−H tautomer, shows noticeable differences with respect to the *cis*−N(9)−H enolic tautomer, reflecting the influence that the protonated N(7) atom has in that case. The properties of the into the in-plane electric dipole moment are also in full agreement with the distribution of the negative and positive electrostatic potential around the respective heterocycles.

Finally, for the six tautomers here studied, the respective deprotonated atoms could be only suggested as potential sites in physicochemical processes mediated mainly by electrostatic interactions (or at least in their initial steps). Nevertheless, to postulate the same sites as chemically reactive toward an electrophilic attack (processes in which the covalent contributions could be important), appears very difficult to us and related to the global chemical reactivity problem. For example, considering the two most stable tautomeric forms, the O(10) atom could be postulated in principle as a site of electrophilic

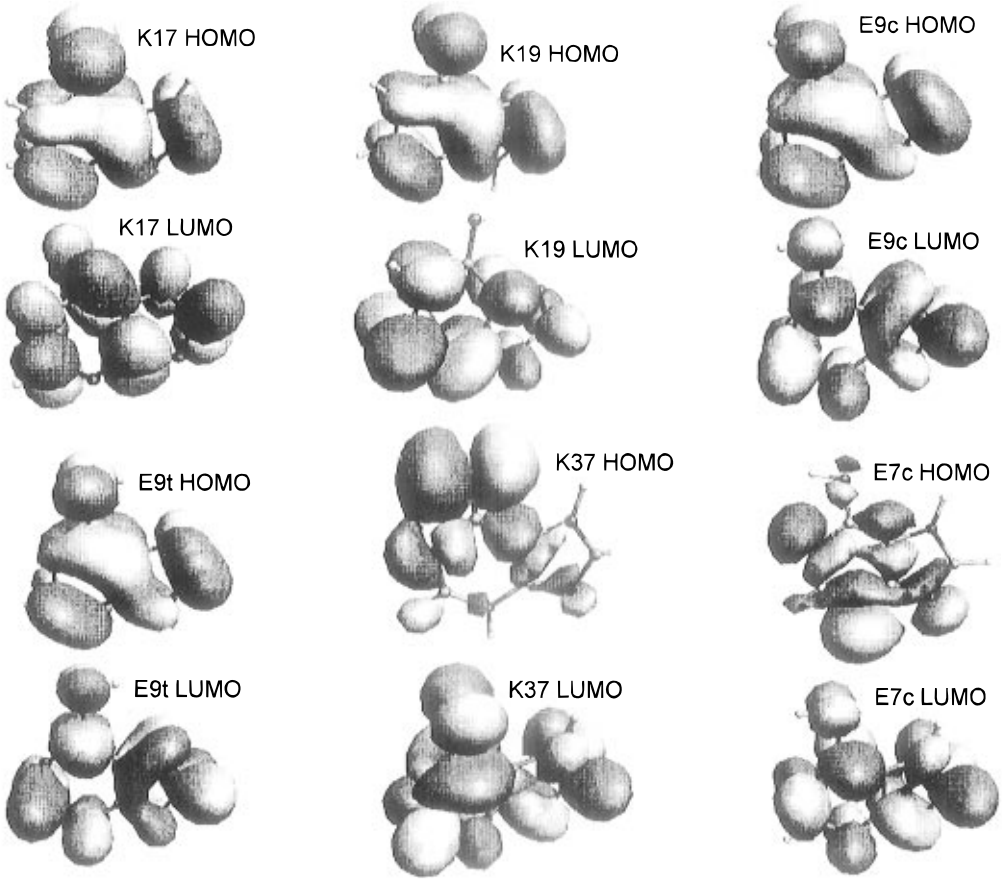

Figure 4. HOMO and LUMO 3-D-wave function (±0.025 level) for the six most stable tautomers.

attack; however, there are no studies reported up to date that show categorically the existence of a direct O(10)−transitional metal chemical bond. The same would be applied for the O(10)−N(7) fragment in the N(1)−H/N(9)−H tautomer, for which there are no reports that show definitively a simultaneous O(10)−transition metal−N(7) chemical bond for this tautomeric form of hypoxanthine. As can be deduced from these examples, many other factors must be considered in the chemical reactivity problem, particularly in condensed phase.

E. Energy and Symmetry Properties of the Wave Function Associated with the Highest Occupied Molecular Orbital and the Lowest Unoccupied Molecular Orbital. Table 2 shows the highest occupied molecular orbital (HOMO) and the lowest unoccupied molecular orbital (LUMO) energies for the six tautomers here studied, and Figure 4 shows the respective 3D-wave function (±0.025 level) associated with the same molecular orbitals.

As can be observed in Figure 4, noticeable trends in the symmetry for the HOMO and LUMO wave functions arise. For the two N(1)−H ketonic and the two N(9)−H enolic tautomers, the symmetry and spatial distribution of the HOMO wave functions are of the same type. From the analysis, a π-type character for the HOMO is deduced, independently of the position of the interchangeable H atoms. It could be suggested that the potential electron donor properties of these four tautomers are nondependent on the positions of the H atoms, and that they are π -type.

For the two less energetically favorable N(7)−H tautomers here studied, the symmetry and spatial distribution properties of their HOMO wave functions are different between them and also with respect to the four above cases: they are σ-type. Here, the σ-type potential electron donor regions are strongly dependent of the interchangeable H atoms positions.

On the other hand, the LUMO wave function is π-type in all the cases. Interestingly, the wave function spatial distribution shows a relative dependence of the interchangeable H atoms, particularly for the case of the N(1)−H ketonic tautomers. For all the tautomers, the potential electron acceptor properties lies upon π-type molecular orbitals.

F. Ionization Potential and Electron Affinity. Table 2 shows the first vertical ionization potential (IP) and the first vertical electron affinity (EA) calculated for each one of the six most stable tautomers of hypoxanthine here studied. These values belong to the processes neutral species → monocationic radical species and neutral species → monoanionic radical species, respectively.

The IP values are in full agreement with the HOMO energy values. A gross increasing trend of the IP values with descending the tautomer energetic stability is observed. The energetically most stable tautomers are associated with relatively lower IP values (*i.e.*, they would be the relatively stronger reductor agents). On the other hand, the experimental spectroscopic vertical IP values for hypoxanthine, to our knowledge and reported up to date, ranges between 8.87 and 8.89 eV.[7,25,26] With respect to the experimental temperature conditions carried out in these experiments, unfortunately only one study[7] makes a detailed description about the temperature at which hypoxanthine in the gas phase was analyzed (T = 530.15 K). This aspect could be important, because as we will show in the next section, the gas-phase temperature influences changes in the relative population of the tautomers. In principle, we think that the experimental signals corresponding to the first IP of hypoxanthine could be weighted by the ionization of the relative tautomeric population in the gas phase at a specific temperature. In fact, in one of the studies, the signal at 8.87 eV and reported as the first IP, is overlapped with a signal at 8.70 eV, this last

being interpreted[26] as the starting of the photoionization. In this way, one can suspect that the experimental signals may be only "iceberg peaks" of very complex processes occurring simultaneously.

The ionization (oxidation) process involves mainly the HOMO of each tautomer, of π-character for the N(1)−H ketonic and the N(9)−H enolic forms, and of σ-type for the N(7)−H tautomers. We have analyzed the possible involvement of other occupied MOs in the first ionization process by looking at the energies of the two most stable tautomers: the nearest occupied MO (σ-type) lies around 0.43 and 0.39 eV below the HOMO energy for the N(1)−H/N(7)−H and the N(1)−H/N(9)−H forms, respectively. This energetic differences let us suspect that this MO could be in some measure involved in the photoionization process of these tautomers. This possibility could have important experimental implications as a consequence of the higher relative population of these two energetically most stable hypoxanthine tautomers in the gas phase.

The theoretical values for the electron affinity are in a general agreement with the LUMO energies for the six most stable tautomers studied. The theoretical value of EA is associated with the relative stability of the tautomer upon a reduction process. In general, the most energetically stable tautomers show higher EA values than the less stable ones (*i.e.*, the more stable ones would be relatively poorer oxidant agents than the less stable ones). Unfortunately, to our knowledge, experimental EA data are not reported up to date.

With respect to the MOs associated with the first EA, we think that the ionization (reduction) process would involve mainly the LUMO of each tautomer of π-type in all the cases. Analyzing the energy of the nearest unoccupied MO, the energy difference between this and the LUMO energy is 0.32 and 0.54 eV for the N(1)−H/N(7)−H and the N(1)−H/N(9)−H forms, respectively. For the other tautomers, this difference increases as the tautomer becomes energetically more unstable. In this way and for the two most stable tautomers, the possible involvement of this unoccupied MO (π-type) in its reduction process could be suspected.

G. Tautomeric Equilibria in Gas Phase as a Function of Temperature. An interesting aspect of the problem about the hypoxanthine tautomers in gas phase lies on the evaluation of the tautomeric equilibrium constants and their behavior with temperature. We calculated the tautomeric constants corresponding to the equilibrium:

$$\text{tautomer N(1)−H/N(7)−H} \rightleftharpoons \text{tautomer } i$$

for which

$$K_{eq} = \frac{[\text{tautomer } i]}{[\text{N(1)−H/N(7)−H}]} = e^{-\overline{\Delta G}/RT}$$

where $\overline{\Delta G}$ is the molar Gibbs free energy difference between tautomer i and N(1)−H/N(7)−H. Table 3 shows the equilibrium constants for all the tautomeric equilibria involving all the possible tautomers of hypoxanthine at three different values of temperature.

As can be seen, the tautomeric constant values at a certain T for the process indicated above follows a trend of descending values, in agreement with the descending energetic stability of tautomer i with respect to the N(1)−H/N(7)−H form. On the other hand, for a specific tautomeric equilibrium, the equilibrium constant shows an increase with temperature. At 298.15 K, the relatively most important tautomeric forms of hypoxanthine in the gas phase would be the two N(1)−H ketonic forms. When increasing the temperature to 480.15 K, the relative contribution of initially unfavorable tautomeric forms shows a significant increase. These results could have important consequences in the analysis of the physicochemical properties experimentally obtained for hypoxanthine in the gas phase at different temperatures.

TABLE 3: Tautomeric Equilibrium Constants at Three Different Temperatures for all the Tautomers in the Gas Phase[a]

tautomer	K_{eq} (T = 480.15 K)	K_{eq} (T = 298.15 K)	K_{eq} (T = 11.0 K)
K19	4.64×10^{-1}	2.85×10^{-1}	1.29×10^{-15}
E9c	1.89×10^{-3}	4.65×10^{-5}	1.31×10^{-116}
E9t	4.79×10^{-4}	5.01×10^{-6}	5.82×10^{-143}
K37	5.47×10^{-4}	4.31×10^{-6}	9.62×10^{-149}
E7c	1.99×10^{-4}	1.12×10^{-6}	3.33×10^{-161}
E3t	2.43×10^{-7}	2.64×10^{-11}	5.40×10^{-286}
E3c	7.52×10^{-8}	3.90×10^{-12}	1.65×10^{-308}
E7t	6.26×10^{-8}	1.47×10^{-12}	0.0
K13	2.75×10^{-9}	1.41×10^{-14}	0.0
E1t	5.93×10^{-10}	1.39×10^{-15}	0.0
K39	1.60×10^{-9}	2.92×10^{-15}	0.0
K79	6.04×10^{-11}	2.91×10^{-17}	0.0
E1c	1.03×10^{-13}	3.59×10^{-22}	0.0

[a] Values correspond to the equilibria N(1)−H/N(7)−H/ ⇌ tautomer i.

H. IR Spectroscopy. As part of the theoretical study of the six tautomers, the calculation of the respective IR vibrational spectrum was carefully done, and the corresponding assignment of the absorptions was carried out. Table 4 shows the corrected wavenumbers, the intensities, and assignment for each one of the absorptions of the theoretical IR vibrational spectrum of the two most stable tautomers of hypoxanthine. As can be deduced from this table, each one of the ketonic tautomers shows characteristic absorptions that can lead to make a detailed comparison with the experimental IR vibrational spectrum of hypoxanthine in gas phase at any temperature below its thermal decomposition. In a previous study,[27] the experimental IR vibrational spectrum of hypoxanthine in an Ar matrix measured by the low-temperature method at 11 K and in the 4000−500 cm^{-1} range was reported. In this, the experimental spectrum was assumed to be mainly a result of the N(1)−H/N(7)−H and N(1)− H/N(9)−H tautomeric contributions. In addition, a small contribution of an enolic tautomer was estimated. This was deduced from the pioneering semiempirical calculations by Pullman *et al.*[4a] on the N(1)−H ketonic tautomers and some others carried out[27] for two enolic forms (N(9)−H and N(7)−H but without detailed information about the OH-group configuration), and from the analysis of the experimental IR data in the 4000−3400 cm^{-1} range of some model heterocycles.

For our theoretical study of the IR vibrational spectrum and its comparison with the experimental one, several assumptions were made: (a) although the experimental IR spectrum was measured at 11 K in an Ar matrix, we considered that at this temperature there are no tautomeric transformations in the solid sample (in fact, the gas mixture freezes at a higher temperature); (b) although the relative population of the hypoxanthine tautomers in the gas phase appears to be dependent on temperature, we assumed that the abrupt decrease of T overcomes the dynamics of the tautomeric equilibria; (c) as a consequence, we considered the experimental sublimation temperature of hypoxanthine[27] (*i.e.*, 480.15 K) as a more realistic value for which the analysis of the relative population of the hypoxanthine tautomers in the gas phase should be done.

From these considerations, the relative population of the hypoxanthine tautomers used to analyze the experimental IR spectrum was the one that corresponds to the tautomeric

TABLE 4: Wavenumbers ($\bar{\nu}$, cm^{-1}), intensities (*I*, kM/mol) and Vibrational Modes Assignment for the Theoretical IR Spectra of the Two Most Stable N(1)−H/N(7)−H and N(1)−H/N(9)−H Ketonic Tautomers

K17			K19		
$\bar{\nu}$	*I*	assignment	$\bar{\nu}$	I	assignment
3504.25	81.41	ν(*N*(7)−H)	3504.93	71.07	ν(*N*(9)−H)
3456.38	57.90	ν(*N*(1)−H)	3453.30	57.17	ν(*N*(1)−H)
3166.94	1.92	ν(*C*(8)−H)	3164.79	0.81	ν(*C*(8)−H)
3094.40	9.96	ν(*C*(2)−H)	3099.68	7.09	ν(*C*(2)−H)
1715.00	652.68	ν(C═O), rings vib, *N*(1)−H vib	1735.53	612.37	ν(C═O), δ (N(1)−H), rings vib
1570.21	63.05	rings vib, *C*(2)−H vib, δ(*N*(1)−H), ν(C═O)	1561.97	88.39	rings vib, *C*(2)−H vib, ν(C═O)
1493.04	19.78	rings vib, *N*(7)−H vib, ν(C═O)	1532.08	51.49	rings vib, *N*(9)−H vib, δ(*C*(8)−H)
1487.36	8.62	rings vib, *C*(2)−H vib	1466.90	20.31	rings vib, *C*(8)−H vib, *N*(1)−H vib, ν(C═O)
1413.32	35.74	rings vib, *C*(8)−H vib, ν(C═O)	1422.19	1.79	rings vib, *N*(1)−H vib, *C*(8)−H vib, ν(C═O)
1377.94	18.71	rings vib, *N*(1)−H/*N*(7)−H vib, ν(C═O)	1377.46	7.40	rings vib, *N*(1)−H vib, *C*(2)−H vib, δ(*N*(9)−H)
1360.70	28.02	rings vib, *C*(2)−H vib, δ(*C*(8)−H)	1350.06	24.85	rings vib, *C*(2)−H vib, *N*(9)−H vib, δ(*N*(1)−H)
1348.05	84.42	rings vib, N−H vib, ν(C═O)	1329.15	34.89	rings vib, *C*(2)−H vib, *N*(1)−H vib
1305.06	18.42	rings vib, *C*(2)−H vib, *N*(7)−H vib, ν(C═O)	1308.39	1.94	rings vib, *C*(2)−H vib, *C*(8)−H/*N*(9)−H vib, ν(C═O)
1246.36	1.08	rings vib, *C*(8)−H vib	1247.29	5.16	rings vib, *C*(8)−H vib, *N*(9)−H vib, *N*(1)−H/*C*(2)−H vib
1155.14	67.99	rings vib, C(8)−H vib, N−H vib	1141.25	68.68	rings vib, *C*(8)−H vib, N−H vib
1078.21	5.14	rings vib, *N*(1)−H vib	1091.60	12.06	rings vib, *N*(1)−H vib
1053.17	46.20	rings vib, *N*(7)−H vib	1037.63	17.21	rings vib, *N*(9)−H vib
1031.23	7.82	rings vib, *N*(7)−H vib, *C*(8)−H vib	1016.49	37.00	rings vib, *C*(2)−H vib, C═O vib
916.17	1.46	rings vib, *N*(7)−H vib, *C*(2)−H vib	903.52	6.19	rings vib, *N*(9)−H vib, *C*(8)−H vib
865.76[a]	10.71	*C*(2)−H vib, pyrimidinic ring vib	864.89[a]	7.26	*C*(2)−H vib, pyrimidinic ring vib
858.11	2.07	rings vib	859.91	8.71	rings vib
793.94[a]	21.14	*C*(8)−H vib, imidazolic ring vib	777.05[a]	17.35	*C*(8)−H vib, rings vib
748.96[a]	0.68	rings vib, *C*(8)−H vib	742.34[a]	13.58	*C*(8)−H vib, rings vib
693.41[a]	32.51	rings vib, N(1)−H vib, C═O vib	694.68[a]	45.86	N(1)−H vib, rings vib
683.99	2.57	rings vib	673.05	10.54	rings vib
643.36[a]	25.12	rings vib, N−H vib	639.14[a]	10.30	*N*(1)−H vib, rings vib
608.37[a]	32.92	rings vib, N−H vib	623.31[a]	12.29	*N*(1)−H vib, rings vib
584.25	5.12	rings vib	579.39	6.84	rings vib,ν(C═O)
533.29[a]	24.48	rings vib, *N*(1)−H vib	535.93[a]	96.70	*N*(9)−H vib, rings vib
522.03	2.05	rings vib	511.53	9.48	rings vib
491.96	2.43	rings vib	488.21[a]	31.79	*N*(9)−H vib, rings vib
489.33[a]	79.82	imidazolic ring vib, *N*(7)−H vib	485.41	1.34	rings vib
290.16	15.48	rings vib, C═O vib	305.76	1.15	rings vib, C═O vib
258.66[a]	6.95	rings vib	249.47[a]	0.09	rings vib
186.49[a]	13.19	rings vib	197.20[a]	19.63	rings vib
147.64[a]	11.35	rings vib, C═O vib	141.33[a]	0.82	rings vib, C═O vib

[a] All the vibrational modes at the indicated wavenumber are out of molecular plane (omp).

equilibria at 480.15 K and for which the equilibrium tautomeric constants have been previously discussed (Section G, Table 3). The respective mole fraction (x_i) of each tautomer was obtained from the K_{eq} values. The theoretical intensities of the absorptions in each spectrum were weighted by the correspondent mole fraction. After this, all the intensities were scaled relative to the signal of highest intensity value. As a result, a theoretical IR spectrum considering the relative contributions of the six most stable tautomers at 480.15 K was obtained. The experimental spectrum was carefully scanned and digitized upon a meticulous comparison with the data in a table reported in ref 27, and the experimental absorptions were also scaled with respect to the highest intensity experimental value. Both spectra, the experimental and the theoretical one, are shown in Figure 5.

From their comparison, a reasonable concordance in both the wavenumber and intensity patterns between several groups of highest absorptions in the two spectra is found. These groups belong to the 3510−3300, 1800−1200, 1100−1000, and 1000−500 cm^{-1} ranges. In order to carry out the spectral characterization of the experimental IR spectrum from a theoretical point of view, we first constructed the theoretical spectrum by the successive incorporation of each tautomer in order of descending energetic stability and made a detailed comparison of the possible changes observed. From this procedure, an essential contribution of the N(1)− H/N(7)−H and N(1)−H/N(9)−H tautomers was found: the resultant theoretical IR spectrum (Figure 5b) and its observable absorptions correspond to the two N(1)−H ketonic tautomers contributions. The energetically less stable tautomers do not show significant spectral contributions to the theoretical IR spectrum plotted in Figure 5b.

Characterization of the Experimental IR Spectrum of Hypoxanthine from the Theoretical Study

A. 3510−3300 cm^{-1} Range. The experimental IR bands with maxima of absorptions at 3464 cm^{-1} (band 1) and 3428 cm^{-1} (band 2) could be assigned to the ν_{N-H} (imidazolic ring) and ν_{N-H} (pyrimidinic ring) vibrational modes, respectively. Although the theoretical wavenumbers for these two vibrational modes in the N(1)−H ketonic tautomers are at slightly higher values than the experimental ones, their relative intensities are very similar. When analyzing in more detail the two experimental bands, a shoulder in both is observed. For the band at 3464 cm^{-1}, a shoulder at 3478 cm^{-1} is detected; for the band at 3428 cm^{-1} a shoulder in the low-energy side is suggested. From the comparison between these two experimental bands and their correspondent theoretical ones, the absorptions at 3464 and 3428 cm^{-1} are attributed, respectively, to $\nu_{N(7)-H}$ and $\nu_{N(1)-H}$ of the N(1)−H/N(7)−H tautomer. The two shoulders of the experimental bands are attributed, respectively, to $\nu_{N(9)-H}$ (the one at higher wavenumber) and $\nu_{N(1)-H}$ (the one at lower energy) of the N(1)−H/N(9)−H tautomer.

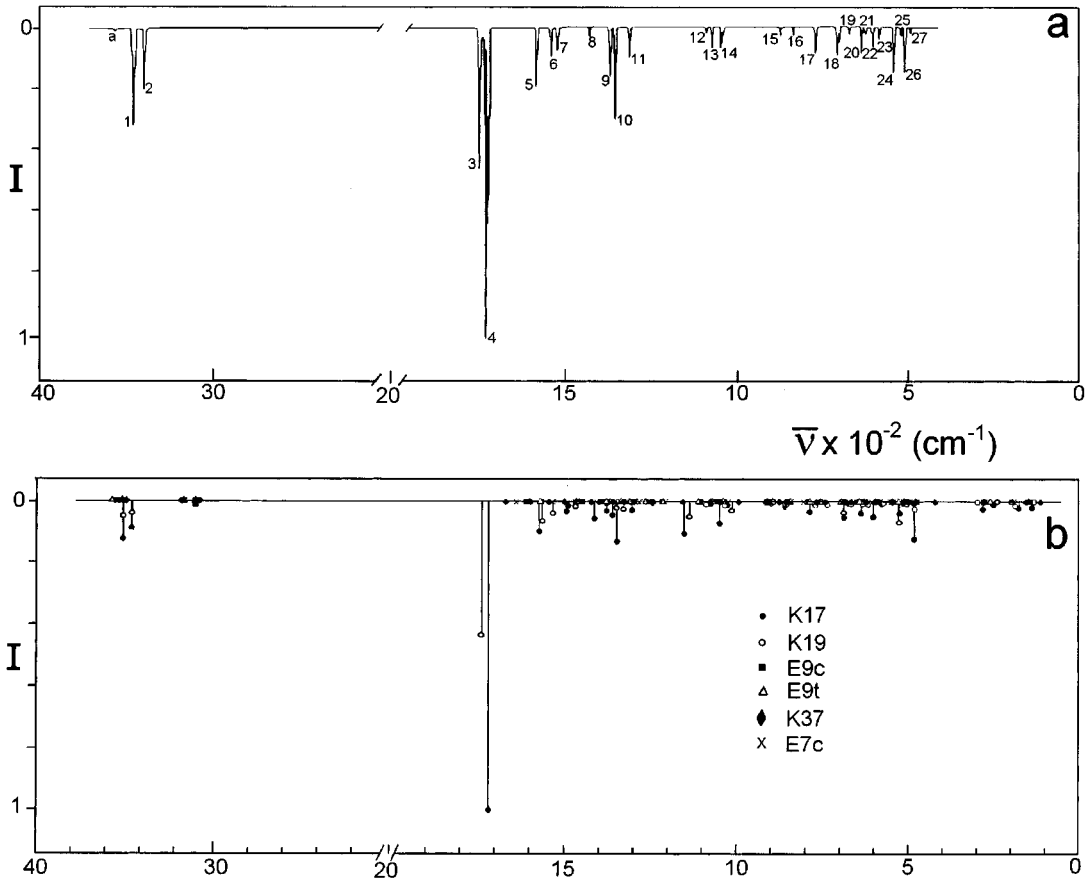

Figure 5. IR vibrational spectra for hypoxanthine (a) experimental (from ref 27), and (b) theoretical (this study).

B. 1800−1200 cm^{-1} Range. The experimental bands at 1753 cm^{-1} (band 3) and 1735 cm^{-1} (band 4) are very similar in wavenumber and relative intensity to two theoretical absorptions of the two N(1)−H ketonic tautomers. Considering the previous assignment of the theoretical absorptions of the N(1)−H ketonic tautomers, it can be proposed that the band at 1753 cm^{-1} is due to the modes νC═O/N(1)−H vib/rings vib of the N(1)−H/N(9)−H tautomer (vib means vibration). The band at 1735 cm^{-1} is attributed to contain the modes νC═O/ rings vib/N(1)−H vib of the N(1)−H/N(7)−H tautomer. In this same range, there are three bands at 1595 cm^{-1} (band 5), 1555 cm^{-1} (band 6), and 1534 cm^{-1} (band 7). Comparing these with the absorptions of the theoretical IR spectrum, the band at 1595 cm^{-1} is associated with the modes rings vib/C(2)−H vib/ N(1)−H vib/νC═O of the N(1)−H/N(7)−H form. The band at 1555 cm^{-1} is attributed to the modes rings vib/C(2)−Hvib/ νC═O, and the one at 1534 cm^{-1} is associated with the modes rings vib/N(9)−H vib/ C(8)−H vib, both of the N(1)−H/ N(9)−H tautomer.

Finally, there are bands in this range appearing at 1433 cm^{-1} (band 8), 1384 and 1381 cm^{-1} (band 9), 1371 cm^{-1} (band 10), and 1324 cm^{-1} (band 11). When comparing them with the theoretical absorptions, for the first we suggest the contribution of the modes rings vib/C(8)−Hvib/νC═O of the N(1)−H/ N(7)−H tautomer; the second one (doublet) is suggested to contain mainly both the modes rings vib/N-H vib/νC═O and the rings vib/C(2)−H vib/ C(8)−H vib of the N(1)−H/N(7)−H form. The band at 1371 cm^{-1} could be associated mainly with the modes rings vib/N-H vib/νC═O of the same tautomer. The band at 1324 cm^{-1} is proposed to contain both the modes rings vib/C(2)−H vib/N(1)−H vib of the N(1)−H/N(9)−H tautomer, and the modes rings vib/C(2)−H vib/N(7)−H vib/νC═O of the N(1)−H/N(7)−H tautomer.

C. 1100−1000 cm^{-1} Range. In this range, the experimental IR spectrum show bands at 1100 cm^{-1} (band 12), 1084 cm^{-1} (band 13), and 1062 and 1054 cm^{-1} (band 14). Again, comparing them with the theoretical spectrum, the following assignment can be suggested: the band at 1100 cm^{-1} corresponds to the modes rings vib/N(1)−H vib of the N(1)−H/ N(9)−H tautomer; the band at 1084 cm^{-1} is attributed to the modes rings vib/N(1)−H vib of the N(1)−H/N(7)−H form, and the band of complex structure with absorptions at 1062 and 1054 cm^{-1} can be assigned, the first one to the modes rings vib/ N(7)−H vib of the N(1)−H/N(7)−H tautomer, and the second one to the modes rings vib/N(imidazolic)−H vib of both N(1)−H ketonic tautomers, without discarding some contribution of the modes C(2)−H vib/C═O vib of the N(1)−H/N(9)−H tautomer.

D. 1000−500 cm^{-1} Range. Several low-intensity bands appear in this range. Comparing carefully the wavenumber and intensity patterns with the theoretical ones, assignment for those was possible. These are as follows (omp means out of the molecular plane): 891 cm^{-1} (band 15), rings vib/N(9)−H vib/ C(8)−H vib of N(1)−H/N(9)−H; 860 cm^{-1} (band 16), C(2)−H vib/pyrimidinic ring vib (omp) of both N(1)−H ketonic tautomers; *ca.* 775 cm^{-1} (band 17), C(8)−H vib/rings vib (omp) of the N(1)−H ketonic tautomers; 725 cm^{-1} (band 18), N(1)−H vib/rings vib (omp) of the N(1)− H ketonic tautomers; 691 cm^{-1} (band 19), rings vib of the N(1)−H ketonic tautomers; 657 cm^{-1} (band 20), rings vib/ N-H vib (omp) of the N(1)−H/N(7)−H tautomer; 640 cm^{-1} (band 21), N(1)−H vib/rings vib (omp) of the N(1)− H/N(9)−H tautomer; 626 and 622 cm^{-1} (band 22), rings vib/ N-H vib (omp) of the N(1)−H ketonic tautomers; 602 and 598 cm^{-1} (band 23), essentially rings vib of the N(1)−H ketonic tautomers; 558 and 553 cm^{-1} (band 24), N(9)−H vib/ rings vib (omp) of the N(1)−H/N(9)−H tautomer and rings vib/

N(1)−H vib (omp) of the N(1)−H/N(7)−H tautomer, respectively; 542 and 534 cm^{-1} (band 25), rings vib of both N(1)−H ketonic tautomers; 524 cm^{-1} (band 26): imidazolic ring vib/ N(7)−H vib (omp) of the N(1)−H/N(7)−H. Finally, the band at 508 cm^{-1} (band 27) is attributed to N(9)−H vib/rings vib (omp) of the N(1)−H/N(9)−H tautomer.

On the other hand, and from the same analysis, our theoretical spectral results let us propose the existence of absorptions in the experimental IR spectrum for the ranges *ca.* 3300−3000 cm^{-1} (for the ν C(8)−H and ν C(2)−H modes of both N(1)−H ketonic tautomers), *ca.* 1520−1450 cm^{-1} (for the rings vib/ N(7)−H vib/ C(2)−H vib/ν C═O modes of the N(1)−H/N(7)−H form), and *ca.* 1200−1100 cm^{-1} (for the rings vib/ C(8)−H vib/N-H vib of both N(1)−H ketonic tautomers). Other theoretical absorptions (their characterization appears in Table 4) are also predicted below 500 cm^{-1}.

From the above analysis, only the vibrational modes of the two N(1)−H ketonic tautomers have significative contributions. On this respect, it is important to raise the point that, in the experimental study,[27] the spectral contribution of an enolic tautomer was established by scaling the total intensity of the spectrum; from this, a band of extremely low-intensity was shown in the original spectrum at 3578 cm^{-1} (band *a* in the experimental spectrum of Figure 5). The authors used some semiempirical results (that predict the existence of this band) and the IR data (4000−3400 cm^{-1}) of some model heterocycles to propose the enolic tautomeric contribution.

We attempted to make noticeable the theoretical absorptions associated with the ν OH mode for the cis- and trans-N(9)−H enolic tautomers in the spectrum of Figure 5, and only when multiplying their intensity by a factor of 100 were they detected. The complexity of the resulting theoretical spectrum made it very difficult to consider that bands associated clearly with vibrational modes of the OH group could be detected in the experimental spectrum. It is then very difficult for us to consider a significative contribution of an enolic tautomer (*i.e.*, the *cis*- or *trans*-N(9)−H, or both) in the experimental IR spectrum of hypoxanthine. These considerations could be in agreement with a mass spectrum study ($T = 525.15$ K) of hypoxanthine,[28] from which the existence of only the N(1)−H ketonic forms was deduced.

IV. Concluding Remarks

In the theoretical study carried out, the total energy, the structural properties, the electronic structures, some properties associated with electrostatic interactions and redox processes, and the IR vibrational spectra of all the ketonic and enolic tautomeric forms of neutral hypoxanthine were calculated. Here, those corresponding to the six energetically most stable tautomers have been shown and discussed. Agreement with the experimental data available for hypoxanthine is remarkable. From this study, the following conclusions can be drawn.

Conclusion 1. The total energy values let us consider the highest relative energetic stability for the two N(1)−H ketonic tautomers, followed by the two enolic N(9)−H, the N(3)−H/ N(7)−H, and the *cis*−N(7)−H enolic forms. For the N(1)−H ketonic tautomers, and at this level of study, the N(1)−H/ N(7)−H form is slightly more stable than the N(1)−H/N(9)−H one.

Conclusion 2. The values of the structural parameters are noticeably sensitive to the tautomeric form. The experimental trend found about the increase of the angle for a specific region in the heterocycles upon a protonation or a metallic coordination has been also obtained here. All the tautomeric forms studied are remarkably planar in isolated form. Interestingly and for the enolic forms, the OH group is also found to be located into the molecular plane. The theoretical values of the same structural parameters, let us consider the existence of endocyclic regions with a double bond character, which are remarkably dependent on the position of the interchangeable H atoms involved in the prototropic tautomerism. For the ketonic forms this same character is attributed to the C(6)−O(10) group.

Conclusion 3. The total electronic density distribution is also noticeably sensitive to the tautomeric form, according to the values of the structural parameters and the Mayer valence indices values.

Conclusion 4. In agreement with the structural parameters, the total electronic density, and the Mayer valence indices, the negative electrostatic potential distribution is also strongly dependent on the tautomeric form: those endocyclic atomic regions involved in double bonds are also associated with very negative potentials. In contrast, all the protonated regions (N−H or C−H groups) are associated with positive potentials. For the exocyclic O atom, the spatial distribution of the negative electrostatic potential is dependent on both the tautomeric form (ketonic or enolic), and for the last one, on its configuration. We also found concordance between the electric dipole moment and the above properties.

Considering all these properties, possible favorable sites for interactions with electrophilic agents which are directed in the first steps (or essentially) by electrostatic contributions can be suggested, being in principle those associated with a higher total electronic density, a very negative electrostatic potential, and the negative end of the electric dipole moment vector. Interestingly and for the N(1)−H ketonic tautomers, the most stables in solution, the metallic coordination behavior found up to date involves mainly those atomic regions with the properties rationalized before: the N(3) and N(9) atoms for the N(1)−H/ N(7)−H form and the N(7) or the N(3) and N(7) atoms for the N(1)−H/N(9)−H. Unfortunately, there are no reports on theoretical and experimental studies where the participation of other less stable tautomers here studied is considered. In spite of the above considerations and experimental evidences, one has to be cautious about the reactivity sites studies in these heterocycles. Many other factors, as for example the kinetic one, can play a critical role.

Conclusion 5. The properties of the wave function associated with the molecular orbitals would appear to have significative contributions and implications in the reactivity of the tautomers (mainly the most stable ones) toward Lewis acids, particularly those having π-type frontier MOs energetically accessible for electron transfer processes. In particular, these results for the most stable tautomers of hypoxanthine, let us propose that in their respective interaction with a transitional metallic center through a specific potential coordination site (*e.g.*, the N(7) atom), the initial step of the chemical bond formation in that site could be feasible although the same N atom shows a σ-bond with an H atom. This would mean that the protonated N atom has not necessarily filled its bonding capacity, and thus it can react with other electrophilic agent. This let us suspect that the initial step of the protonated N atom−transition metal chemical bond formation does not necessarily require the respective N atom protonic dissociation. In other words, the potential reactivity of an specific N atom towards a transitional metallic center does not require its existence in a deprotonated form.

Conclusion 6. From the first IP and EA theoretical values, an approximated both increasing trend for the first one and decreasing for the second one, with descending energetic stability of the tautomers is found. These properties could have

significative consequences in the reactivity of the N(1)−H ketonic forms, because they would be the strongest reductors (*i.e.*, weakest oxidants) tautomers. For these two tautomers, the electron donor-acceptor properties are associated with the π-type frontier MOs, but without excluding the possible contribution of the respective energetically nearest MO for each one of those.

Conclusion 7. The theoretical tautomeric equilibrium constants calculated for the whole set of tautomers at different temperatures show a decreasing tendency for the relative contribution of the energetically less stable tautomeric forms with the temperature decrease. The equilibrium constants at the sublimation temperature ($T = 480.15$ K) were used to obtain the relative contribution of the tautomers to the theoretical IR vibrational spectrum. The theoretical spectral analysis carefully carried out has lead to the characterization of the absorptions of the experimental IR data, being the N(1)−H ketonic tautomers the spectroscopically observable ones. In our opinion, the enolic tautomers (*e.g.*, the N(9)−H forms) have no significative contributions at this spectroscopic level and for the thermal conditions considered.

Finally, the highest energetic stability of the N(1)−H ketonic tautomeric forms here found would appear to be in correspondence with their clear spectroscopic preponderance in solution studies. Comparing the relative population of the N(1)−H/N(7)−H and N(1)−H/N(9)−H tautomers, both in solution and in gas phase, the environment dielectric properties influence is clear: the tautomeric form with higher electric dipole moment shows an increasing contribution in the relative population as the environment dielectric constant increases, as in the case of the N(1)−H/N(9)−H ketonic tautomer.

Acknowledgment. The authors are indebted to DGSCA-UNAM and UAM-Iztapalapa for the computer service facilities. We also acknowledge Dr. Alberto Vela (UAM-I) for his advice on some aspects of the calculations.

Supporting Information Available: Internuclear distances, angles, and 3-D electrostatic potentials (−20 kcal/mol) for the six most stable tautomers and vibrational modes assignment to the theoretical IR spectra for four tautomers (9 pages). Ordering information is given on any current masthead page.

References and Notes

(1) For example, see: (a) Hughes, M. N. *The Inorganic Chemistry of Biological Processes*, 2nd ed.; John Wiley & Sons: New York, 1981. (b) Stryer, L. *Biochemistry*, 3rd ed.; Freeman: New York, 1988. (c) *Nucleic Acid-Metal Ion Interactions*; Spiro, T. G., Ed., John Wiley & Sons: New York, 1980; Vol. 1. (d) Lusty, J. R., Ed. *CRC Handbook of Nucleobase Complexes*; CRC Press: Boca Raton, FL, 1990; Vol. I. (e) Kwiatkowski, J. S.; Zielinski, T. J.; Rein, R. in *Advances in Quantum Chemistry;* Löwdin, P. O., Ed.; Academic Press, Inc.: New York, 1986; Vol. 18, p 85.

(2) Tauler, R.; Cid, J. F.; Casassas, E. *J. Inorg. Biochem.* **1990**, *39*, 277.

(3) Acevedo-Chávez, R.; Costas, M. E.; Escudero, R. *Inorg. Chem.* **1996**, *35*, 7430.

(4) (a) Pullman, B.; Pullman, A. *Adv. Heterocycl. Chem.* **1971**, *13*, 77. (b) Lichtenberg, D.; Bergmann, F.; Neiman, Z. *Isr. J. Chem.* **1972**, *10*, 805. (c) Chenon, M. T.; Pugmire, R. J.; Grant, D. M.; Panzica, R. P.; Townsend, L. B. *J. Am. Chem. Soc.* **1975**, *97*, 4636.

(5) (a) Cheng, D. M.; Kan, L. S.; Ts'o, P. O. P.; Prettre, C. G.; Pullman, B. *J. Am. Chem. Soc.* **1980**, *102*, 525. (b) Szczepaniak, K.; Szczespaniack, M. *J. Mol. Struct.* **1987**, *156*, 29. (c) Person, W. B.; Szczepaniak, K.; Szczespaniack, M.; Kwiatkowski, J. S.; Hernández, L.; Czerminski, R. *J. Mol. Struct.* **1989**, *194*, 239. (d) Nowak, M. J.; Lapinski, L.; Kwiatkowski, J. S. *Chem. Phys. Lett.* **1989**, *157*, 14. (e) Santhosh, C.; Mishra, P. C. *Spectrochim. Acta* **1993**, *A49*, 985.

(6) Neiman, Z. *Isr. J. Chem.* **1971**, *9*, 119.

(7) Lin, J.; Yu, C.; Peng, S.; Akiyama, I.; Li, K.; Lee, L. K.; LeBreton, P. R. *J. Phys. Chem.* **1980**, *84*, 1006.

(8) Aaron, J. J.; Gaye, M. D.; Párkányi, C.; Cho, N. S.; Von Szentpály, L. *J. Mol. Struct. (THEOCHEM)* **1987**, *156*, 119.

(9) Ohta, Y.; Nishimoto, K.; Tanaka, H.; Baba, Y.; Kagemoto, A. *Bull. Chem. Soc. Jpn.* **1989**, *62*, 2441.

(10) Leo, T.; Accion, F.; Escolar, D.; Tortajada, J. *An. Quim.* **1991**, *87*, 14.

(11) Nonella, M.; Hänggi, G.; Dubler, E. *J. Mol. Struct. (THEOCHEM)* **1993**, *279*, 173.

(12) El-Bakali Kassimi, N.; Thakkar, A. J. *J. Mol. Struct. (THEOCHEM)* **1996**, *366*, 185.

(13) Lazo, L.; Tejo, A. M.; Pousa, J. L.; Sorarrain, O. M.; Roncaglia, H. A. *Z. Phys. Chemie* (*Leipzig)* **1985**, *266*, 143.

(14) Sheina, G. G.; Stepanian, S. G.; Rádchenko, E. D.; Blagoi, Yu.P. *J. Mol. Struct. (THEOCHEM)* **1987**, *158*, 275.

(15) Hernández, B.; Luque, F. J.; Orozco, M. *J. Org. Chem.* **1996**, *61*, 5964.

(16) Becke, A. D. *Phys. Rev. A* **1988**, *38*, 3098.

(17) Perdew, J. P. *Phys. Rev. B* **1986**, *33*, 8822.

(18) Godbout, N.; Salahub, D. R.; Andzelm, J.; Wimmer, E. *Can. J. Chem.* **1992**, *70*, 560.

(19) Frisch, M. J.; Trucks, G. W.; Schlegel, H. B.; Gill, P. M. W.; Johnson, B. G.; Robb, M. A.; Cheeseman, J. R.; Keith, T.; Petersson, G. A.; Montgomery, J. A.; Raghavachari, K.; Al-Laham, M. A.; Zakrzewski, V. G.; Ortiz, J. V.; Foresman, J. B.; Cioslowski, J.; Stefanov, B. B.; Nanayakkara, A.; Challacombe, M.; Peng, C. Y.; Ayala, P. Y.; Chen, W.; Wong, M. W.; Andres, J. L.; Replogle, E. S.; Gomperts, R.; Martin, R. L.; Fox, D. J.; Binkley, J. S.; Defrees, D. J.; Baker, J.; Stewart, J. P.; Head-Gordon, M.; Gonzalez, C.; Pople, J. A. *Gaussian 94*, Revision D.4; Gaussian, Inc.: Pittsburgh, PA, 1995.

(20) Schmalle, H. W.; Hänggi, G.; Dubler, E. *Acta Crystallogr.* **1988**, *C44*, 732.

(21) Frisch, M. J.; Trucks, G. W.; Schlegel, H. B.; Gill, P. M. W.; Johnson, B. G.; Wong, M. W.; Foresman, J. B.; Robb, M. A.; Head-Gordon, M.; Replogle, E. S.; Gomperts, R.; Andres, J. L.; Raghavachari, K.; Binkley, J. S.; Gonzalez, C.; Martin, R. L.; Fox, D. J.; Defrees, D. J.; Baker, J.; Stewart, J. J. P.; Pople, J. A. *Gaussian 92/DFT*, Revision F.3; Gaussian, Inc.: Pittsburgh, PA, 1993.

(22) UNICHEM 3.0, Cray Research, Inc., 1995.

(23) DGAUSS 3.0.1/UC-3.0, Cray Research, Inc.

(24) Mayer, I. *Int. J. Quantum Chem.* **1986**, *29*, 477.

(25) Hush, N. S.; Cheung, A. S. *Chem. Phys. Lett.* **1975**, *34*, 11.

(26) Dougherty, D.; Younathan, E. S.; Voll, R.; Abduluur, S.; McGlynn, S. P. *J. Electron Spectrosc. Relat. Phenom.* **1978**, *13*, 379.

(27) Sheina, G. G.; Stepanian, S. G.; Rádchenko, E. D.; Blagoi, Yu. P. *J. Mol. Struct. (THEOCHEM)* **1987**, *158*, 275.

(28) Rice, J. M.; Dudek, G. O. *J. Am. Chem. Soc.* **1967**, *89*, 2719.